Nonlocal inverse design of an ultrasonic lens for underwater manipulation of orbital angular momentum

Chuanxin Zhang[1,‡] Fei Dai,[1,‡] Xue Jiang[1,2,*] and Dean Ta[1,2,†]

[1]*Department of Biomedical Engineering, School of Information Science and Technology, Fudan University, Shanghai, 200433, China*

[2]*State Key Laboratory of Integrated Chips and System, Fudan University, Shanghai, 200433, China*

Acoustic orbital angular momentum (OAM) beams hold potential for underwater communications, particle manipulation, and biomedical applications. However, adapting air-based OAM technologies to the underwater environment presents unique challenges. In the underwater environment, the medium cannot be considered acoustically soft, and commonly used ultrasound frequencies have shorter wavelengths compared with air, necessitating new design approaches. Conventional underwater ultrasonic lens design methods often rely on simplified models that neglect nonlocal interactions and diffraction within the structure, therefore leading to suboptimal performance. We introduce a novel nonlocal inverse design method by integrating the full-wave models with the nondominated sorting genetic algorithm II (NSGA-II). This approach diverges from conventional phase-based design by optimizing the physical structure of the lens to account for nonlocal interactions within the material. We experimentally demonstrate the performance when generating high-purity OAM beams underwater. Our experimental results show that this method can generate high-purity OAM beams underwater, achieving over 90% purity for the OAM beams of topological charges from $m = 1$ to $m = 4$. This is a significant improvement compared with traditional methods, which typically reach 70–89% purity. These findings highlight the practical applicability of our method for nonlocally designing the ultrasonic lens, paving the way for advancements in beam performance for various applications.

I. INTRODUCTION

Acoustic orbital angular momentum (OAM) is a rapidly developing field in acoustics with many potential applications, such as high-capacity wireless communication [1–3], precise manipulation of minute particles [4,5], and enhanced medical imaging techniques [6]. OAM beams possess unique helical wave fronts and a property called orthogonality. This allows them to carry separate data streams without interference, a concept known as OAM multiplexing [7,8]. This capability is promising for environments where traditional methods are less effective [9–11], such as underwater communication. Electromagnetic waves weaken rapidly underwater, making long-distance transmission impractical. In addition, acoustic waves experience less dissipation underwater compared with electromagnetic waves, making them suitable for long-range communication. The use of high-purity OAM beams in underwater acoustics holds particular promise

for boosting communication speeds [12]. This is especially crucial for applications like underwater sensor networks, autonomous underwater vehicles, and marine research, all of which heavily rely on robust and high-capacity communication.

Beyond communication, OAM beams offer exciting possibilities for manipulating particles within a fluid, expanding the scope of traditional acoustic applications [13–15]. This targeted manipulation is crucial in scenarios such as drug delivery and microscale assembly, where precise control over minute particles is essential. The underwater environment shares many similarities with the human body, making these advancements relevant for biomedical applications. For example, incorporating OAM beams into medical ultrasound could lead to more targeted and efficient drug delivery systems, as well as improved imaging techniques [6,16–18]. In these contexts, precise manipulation of OAM can significantly enhance the effectiveness of treatments and diagnostics compared with traditional methods.

The potential benefits of OAM technology are particularly notable for underwater applications. However, effectively deploying OAM underwater hinges on

---

*Contact author: xuejiang@fudan.edu.cn
†Contact author: tda@fudan.edu.cn
‡These authors contributed equally to this work

generating high-purity beams. While OAM has seen success for airborne sound [19,20], adapting it to underwater ultrasound presents significant challenges. The distinct acoustic properties of water and ultrasound, including higher velocities, impedances, and shorter wavelengths, make traditional air-based methods like phased arrays and metasurfaces less effective underwater [21]. Phased array systems, for example, become considerably more complex when adapted for high-frequency underwater applications. Similarly, metasurfaces [22] cannot be directly applied underwater due to the need to address acoustic-solid coupling and internal wave diffraction, which are critical underwater but negligible in air [23–25]. In addition, the high precision required for manufacturing underwater ultrasound devices adds complexity when producing these intricate structures. These limitations highlight the difficulty of directly translating air-based OAM models underwater, which necessitates cost-effective, easily manufacturable solutions that offer robust capabilities for manipulating acoustic fields underwater.

In this context, treating the generation of OAM as a specific pattern to be achieved through acoustic holographic lenses [26] presents a promising solution. Such underwater ultrasonic lenses offer a promising alternative for precisely manipulating ultrasound fields underwater. These lenses achieve the desired phase changes in the transmitted beam by modulating their thickness, allowing enhanced control over the acoustic field, and fostering the development of advanced applications. However, conventional design models for these lenses typically rely on oversimplified one-dimensional waveguide models, as shown in Fig. 1(c), which fails to capture the nonlocal interactions [23,27] and diffraction phenomena that occur within the actual lens structure. This limitation undermines their effectiveness in practical underwater applications, particularly for OAM beams where uniform radiation is crucial. Traditionally, these lenses are designed based on theoretical phase requirements without considering the practicalities of implementation. This would lead to suboptimal performance. In practical applications, the fabricated structure is what truly matters. Oversimplified models that do not account for the actual geometry and physical interactions within the lens can significantly reduce the purity of the generated beams, thereby limiting their functionality and potential applications.

To address these limitations, the design process needs to shift from idealized phase design to focus on structure design. This new design process should accurately reflect real-world conditions to achieve optimal performance. Moreover, this shift also requires a transition from a direct design methodology based on theoretical formulas to an inverse design methodology [28–31]. Direct design methods are limited in accounting for structural complexities, while inverse design approaches excel in solving complex problems where the relationship between design parameters and desired outcomes lacks well-defined relationships. Inverse design methods have been widely used across various engineering fields to solve previously intractable problems [27,32].

This study introduces a novel nonlocal inverse design methodology that aims to achieve the actual structure configuration by constructing the full-wave models, which account for the intricate interaction and wave diffraction within the structure and the background medium. By refining radiation control through comprehensive structural optimization, this method improves the quality of OAM beams generated underwater. This transition from simplistic phase models to detailed structural optimizations not only improves beam purity but also broadens the practical applicability of OAM technologies in challenging underwater environments. Our approach utilizes the non-dominated sorting genetic algorithm II (NSGA-II) [33] in conjunction with full-wave models to optimize the design of ultrasonic lenses. By introducing both the coefficient of variation (C) and signal-to-noise ratio (SNR) as key performance metrics, we demonstrate that the inverse-designed OAM beams exhibit superior uniformity and minimal crosstalk. Experimental results show that the purity of non-locally designed OAM beams achieves over 90% across all tested beam orders. This is a significant improvement compared with the 70–89% purity achieved with traditional methods. This enhancement observed in experimental validations underscores the practical applicability and effectiveness of our methodology in real-world scenarios. This comprehensive optimization framework establishes a new standard for designing and deploying OAM technologies, paving the way for advanced acoustic applications in underwater environments.

II. METHOD

A. Nonlocal inverse design methodology

Figure 1(a) showcases a schematic diagram of the nonlocal inverse design methodology. Unlike traditional methods that focus on achieving a desired phase profile, our approach directly optimizes the physical structure of the ultrasonic lens. Traditionally, the ideal phase profile required for an underwater OAM beam was directly calculated from formulas, and then an ultrasonic lens was designed to approximate this phase profile as closely as possible. As illustrated in Fig. 1(c), this approach relies on oversimplified models that assume a direct link between thickness and phase. However, these models fail to capture the intricate interactions and how ultrasound waves diffract within the actual lens structure. These limitations often lead to suboptimal performance because the fabricated lens deviates from the theoretical model, introducing significant errors that degrade beam quality in practical applications. On the contrary, our nonlocal inverse design method overcomes this issue. By integrating full-wave
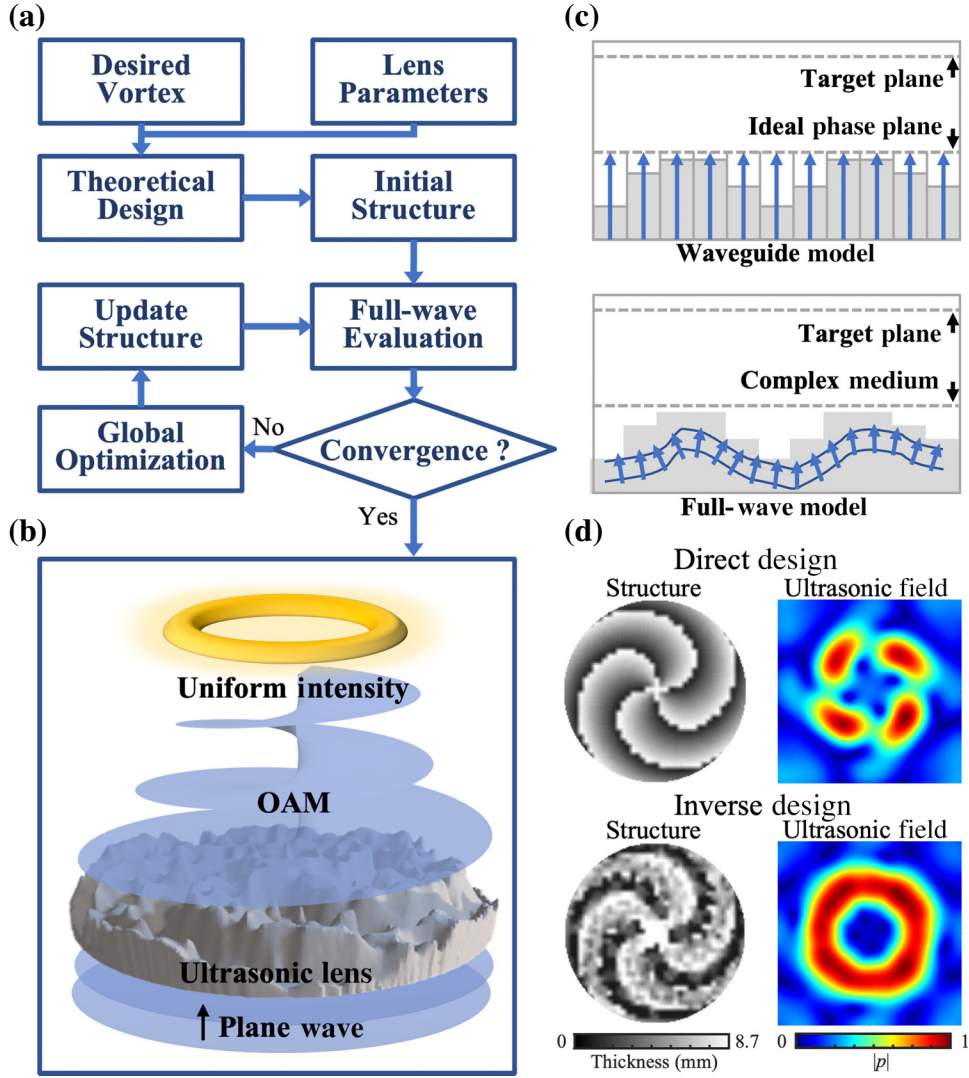
FIG. 1. Nonlocal design of the ultrasonic lens for generating high-quality OAM beam underwater. (a) A schematic diagram of the nonlocal inverse design methodology that directly integrates the structural configurations into the optimization process. (b) A diagram of the inverse-designed ultrasonic lens producing high-quality and focused OAM beams, which is the output result of (a). (c) A comparison that highlights the limitations of conventional designs based on one-dimensional waveguide models, in contrast to the full-wave model that accounts for the nonlocal interaction and wave diffraction within the structure. (d) Comparisons of the lens structure designed with traditional and our methods, along with their resulting ultrasound field distributions.

models, we can account for these complex interactions and diffraction phenomena, ensuring that the designed ultrasonic lens performs effectively underwater. The resulting inverse-designed lens structure, as shown in Fig. 1(b), is optimized to generate high-purity OAM beams, which is evident by its superior beam profile compared with the traditional design [Fig. 1(d)].

B. Initialization

To expedite convergence in the inverse design process, we initialize the lens structure using the traditional direct design method rather than random configurations. The OAM beam has a helical phase profile associated with the azimuthal angle φ. To generate a vortex beam of topological order m at a distance F, the theoretical phase profile on the emitting plane is determined by the following formula:

$$\varphi_{\text{OAM}}(x,y,\ z=0) = k\ \sqrt{x^2+y^2+F^2} + m\varphi, \quad (1)$$

where k is the wave number in free space and $\varphi = \text{Arg}(x+iy)$ is the azimuthal angle in a polar coordinate system.

The simplified waveguide model assumes that the local phase change $\Delta\varphi(x,y)$ is linearly determined by the thickness $T(x,y)$ of the lens [Fig. 1(c)], as described by the

formula [26]:

$$\Delta\varphi(x,y) = T(x,y)(k_h - k_m), \tag{2}$$

where k_h and k_m represent the ultrasound wave numbers in the ultrasonic lens and background medium, respectively. This initial thickness profile $T(x, y)$ is fed into our nonlocal inverse optimization process. To simulate how ultrasound waves propagate through the ultrasonic lens, we utilize the finite-difference time-domain (FDTD) calculation. This calculation is particularly efficient when combined with angular spectrum methods. We perform these simulations using K-WAVE software [34,35], which allows for detailed modeling of ultrasound wave behavior in complex materials. The time-domain simulations run for a duration sufficient to reach a steady state, ensuring accurate results. Finally, we extract the amplitude and phase information of the ultrasound field from the last few cycles of the time signal.

C. Quality evaluation of the OAM beams

After forward-propagation calculations yield the acoustic field distribution at the target plane, we proceed with a comprehensive quality evaluation based on two key metrics: coefficient of variation (C) and signal-to-noise ratio (SNR). These metrics are essential for evaluating the performance and applicability of the beams in different contexts, such as particle manipulation and data communication underwater.

C is defined as the ratio of the standard deviation (σ) to the mean value (μ) of the acoustic pressure, which measures the uniformity of the field, as described by the following:

$$\sigma = \sqrt{\frac{1}{2\pi} \int_0^{2\pi} (|p(r_{\max}, \varphi)| - \mu)^2 \, d\varphi}, \tag{3}$$

$$\mu = \frac{1}{2\pi} \int_0^{2\pi} |p(r_{\max}, \varphi)|^2 \, d\varphi, \tag{4}$$

$$C = \sigma/\mu. \tag{5}$$

Here, $r_{\max}$ denotes the radius with the maximum ultrasound intensity. The SNR quantifies the purity of the OAM beam by comparing the power in the desired m mode to the power in the other $l \neq m$ modes. This is calculated by transforming the ultrasound field into the angular spectrum. The angular spectrum $A(r, l)$ is determined by [36]

$$\frac{1}{2\pi} \int_0^{2\pi} e^{il\varphi} e^{il'\varphi} \, d\varphi = \begin{cases} 1, & l = l' \\ 0, & l \neq l' \end{cases}, \tag{6}$$

$$A(r,l) = \int_0^{2\pi} p(r,\varphi)e^{-il\varphi} \, d\varphi. \tag{7}$$

The SNR is then calculated as

$$\mathrm{SNR} = \frac{\int_0^{r_{\max}} |A(r,m)|^2 r \, dr}{\sum_{l \neq m} \int_0^{r_{\max}} |A(r,l)|^2 r \, dr}. \tag{8}$$

A lower C value indicates a more uniform field distribution, and a higher SNR shows lower crosstalk between different OAM modes, reflecting higher purity and effectiveness of the beam.

Both C and SNR are crucial for achieving high-quality OAM beams. Focusing on only one metric can lead to suboptimal results, such as nonconvergence or entrapment in local minima [37]. Therefore, we use a multiobjective optimization strategy. This approach balances these parameters, ensuring robust and efficient OAM beam generation suitable for various applications.

D. Global optimization algorithm and integration with a full-wave model

To address the multiobjective optimization requirements, we employ the nondominated sorting genetic algorithm II (NSGA-II). NSGA-II is a well-established method for finding the optimal solution to complex optimization problems with multiple competing objectives. It works by creating a pool of potential lens designs and iteratively refining them. By sorting the population of potential solutions into nondominated fronts and maintaining diversity in the population through a crowding distance mechanism, this method explores all possibilities and prevents being stuck on suboptimal solutions.

Designing these lenses is inherently complex due to their three-dimensional structures and nonlocal interactions. To address this, we integrate NSGA-II with full-wave models. The process begins with an initial lens design based on a traditional direct design method. We use FDTD simulations to predict ultrasound wave propagation through the lens, taking into account five constraints: (i) the ultrasound frequency is set at 500 kHz, (ii) the spatial resolution of the lens is 1 mm due to the precision of 3D printing technology, (iii) the computational grid is set at 0.25 mm with remeshing to match the lens and computational grids, (iv) the lens thickness is constrained between 0.25 mm and 8.75 mm, allowing for a 2π-phase change while ensuring manufacturability, and (v) the optimization loop runs for a fixed number of 1,000 iterations, balancing computational efficiency and quality results. Graphics processing unit (GPU) acceleration is employed to parallelly calculate the ultrasound propagation within the structure, and the angular spectrum method is used when calculating the field outside the structure in free space. Following the full-wave simulation, NSGA-II iteratively optimizes the structure parameters. Each new lens design undergoes full-wave simulation to evaluate the resulting OAM beam quality based on C and SNR values.

E. Optimization loop

1. **Initialization.** The process begins with an initial lens structure designed using traditional methods. This initial design is then used to create the starting population by adding random thickness distributions.

2. **Simulating sound waves.** FDTD simulations predict the propagation of ultrasound waves through the initial design, resulting in the acoustic field distribution at the focal plane. Constraints include an ultrasound frequency of 500 kHz, lens spatial resolution of 1 mm, and a computational grid of 0.25 mm. The GPU acceleration and angular spectrum methods are employed.

3. **Evaluating beam quality.** The uniformity (C) and purity (SNR) of the ultrasound beam are assessed. C measures the uniformity of the acoustic field, while SNR quantifies the purity of the OAM beam by comparing the desired mode's power to the power in other modes.

4. **Optimizing with NSGA-II.** Genetic operators, including mutation and crossover, are applied to modify the lens structure based on the evaluation results. The lens thickness is constrained between 0.25 mm and 8.75 mm to allow for a 2π-phase change while ensuring manufacturability.

5. **Repeating the process.** Steps 2–4 are repeated for 1,000 iterations, ensuring the highest quality OAM beam with the best possible C and SNR values.

By combining the power of FDTD simulations, which can accurately predict sound wave behavior, with the optimization capabilities of NSGA-II, we can design and refine complex lens structures for optimal acoustic performance. This combined approach overcomes the limitations of traditional methods that fail to consider the crucial factors of how ultrasound nonlocally interacts with the lens material and background medium. This innovative methodology allows for a more precise and effective design process, ultimately resulting in higher-quality OAM beams that are better suited for real-world underwater applications.

III. RESULTS

To verify the effectiveness of our nonlocal inverse design method in addressing practical challenges, we conducted experiments at 500 kHz using an ultrasound source (piezoelectric transducer) with a diameter of 38 mm. We first measured the ultrasound field without a lens to set the incident boundary condition for our inverse design process. We used a photosensitive resin (mass density 1.180 g/cm^3; and sound speed 2250 m/s) to fabricate the ultrasonic lenses. These material properties are crucial for accurately simulating the nonlocal interaction and were incorporated into our design process. We compared the performances of the traditional direct and our inverse design methods by designing the ultrasonic lenses to generate the OAM beams from $m = 1$ to $m = 4$. We focused these beams on a specific plane at a distance of 40 mm away from the lens along the vertical axis. As shown in Fig. 2, the final lens structures generated by the direct and inverse design methods are illustrated.

The experimental setup is illustrated in Fig. 3. We ensured precise alignment by carefully mounting the lens onto the transducer using a clamp. We also applied vacuum silicone grease between the ultrasonic lens and the transducer to create a tight seal and prevent air gaps that might disrupt ultrasound transmission. The ultrasound pressure distributions at the focus plane were meticulously recorded using a hydrophone (Precision Acoustic, NH0500, 0.5 mm in diameter). This hydrophone was maneuvered by a 3D scanning stage with 1-mm spacing between each point. The temporal signals captured by the hydrophone were analyzed with a Fourier transform to extract the amplitude and phase information of the ultrasound wave. This setup
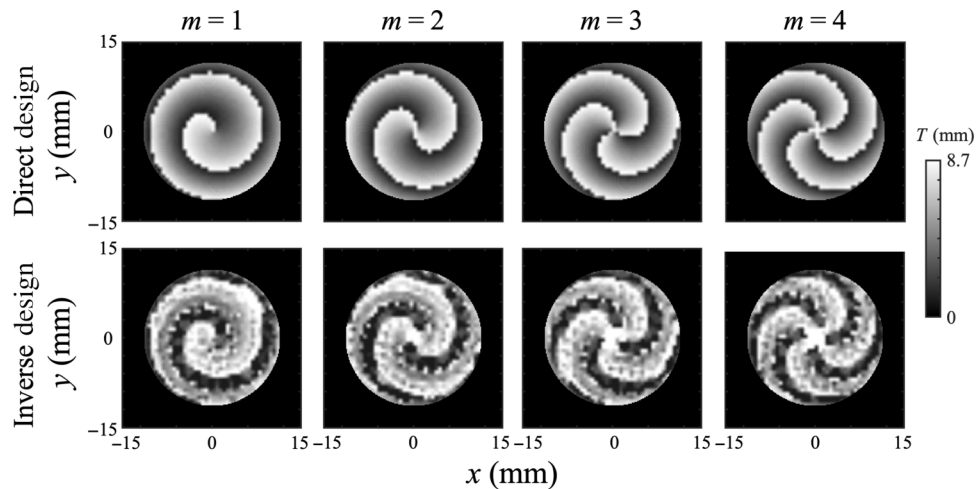

FIG. 2. Thickness profiles of the lenses designed with the direct and nonlocal inverse design methods.
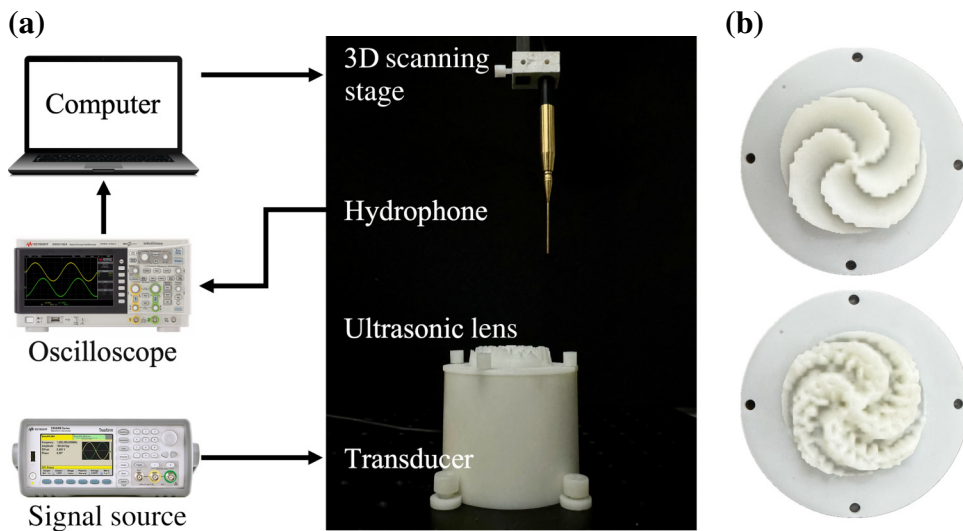
FIG. 3. Schematic of underwater ultrasound field scanning system. (a) A piezoelectric transducer and an ultrasonic lens are used to generate OAM beams. A hydrophone is mounted on a 3D scanning stage to measure the ultrasound pressure distribution. (b) Photographs of ultrasonic vortex lenses ($m = 4$) designed with direct and nonlocal inverse methods.

allowed for precise measurements and analysis of the lens performance in generating OAM beams.

Figure 4 visually compares the performance of lenses designed with a traditional direct and our inverse design methods for different OAM beams. This figure shows the ultrasound field on the focal plane, highlighting the clear improvement achieved with our nonlocal design method.
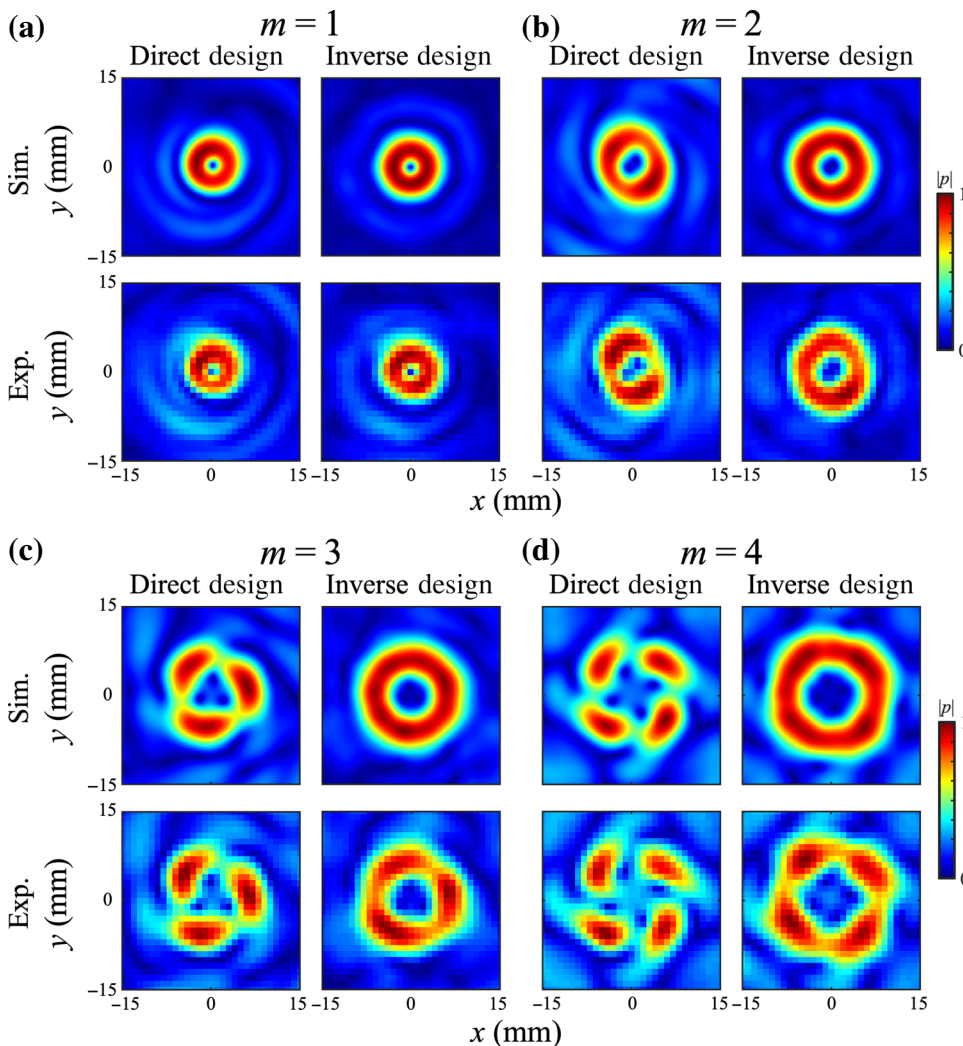

FIG. 4. Comparison of the ultrasound OAM beams generated with the direct and nonlocal inverse design methods in both simulations and experiments. (a)–(d) OAM beams with the topological order m from 1 to 4.

The direct design method employs formulas to program the desired wave front onto the ultrasonic lenses. However, this method ignores the actual structure of the lens, leading to nonuniform intensity across the beam. The resulting ring-shaped intensity patterns resemble fragmented rings with extreme pressure peaks at regular intervals correlated with the OAM beam order. This critical issue arises because the actual thickness of the lens cannot perfectly match the ideal phase profile required for uniform rings. This mismatch causes errors in ultrasound radiation, resulting in the cyclical appearance of extreme values. These findings clearly demonstrate that the uneven beam patterns stem from inherent limitations in the lens structure.

In contrast, our nonlocal inverse design method employs full-wave models to directly optimize the lens structure itself, rather than the ideal phase profile. This approach considers the nonlocal complex interactions between different parts of the lens structure, which are critical for OAM beam performance. By targeting the optimization of structural configurations as the primary object, this method significantly reduces radiation errors caused by inherent structural design factors. This results in beams with highly uniform intensity distributions, which are characterized by smoother transitions and fewer fluctuations in the ultrasound field distribution. The enhanced uniformity achieved with our method is not just theoretical. It has practical implications for applications that rely on precise control of ultrasound waves, such as particle manipulation underwater.

Figure 5 compares the OAM spectra for both direct and inverse designs, which are obtained from simulations and experimental results. These spectra are derived by decomposing the ultrasound field into constituent OAM components using Eq. (7). Each graph represents a specific
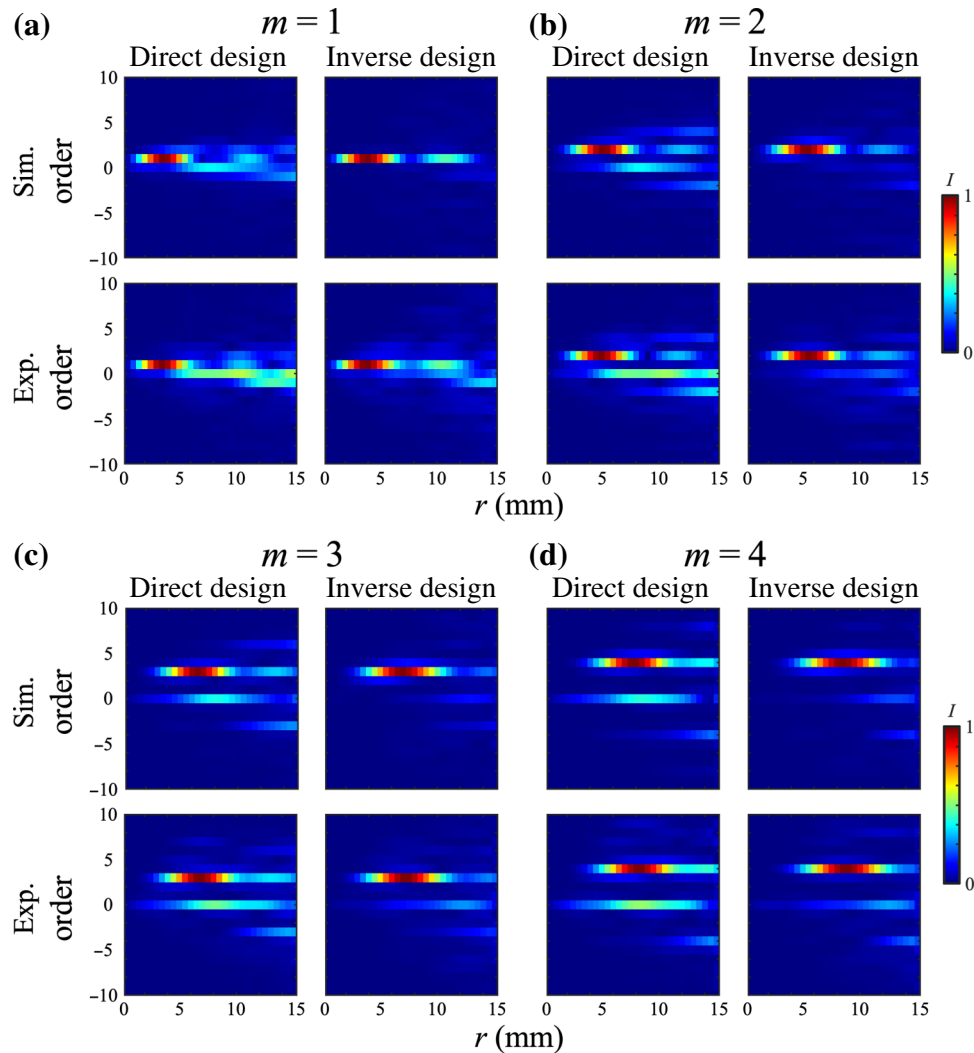

FIG. 5. Comparison of the OAM spectra generated with the direct and nonlocal inverse design methods from both simulations and experiments. (a)–(d) OAM beams with the order m being 1 to 4. The horizontal axis is the radial distance from the beam center, the vertical axis is the OAM order, and the color indicates the strength of specific OAM components.

OAM beam order (m from 1 to 4). The horizontal axis represents the radial distance from the beam center and the vertical axis shows the OAM order. The color indicates the strength of a specific OAM component. Ideally, each graph should show a single dominant peak at the intended OAM order and low intensity for all the other orders; this indicates a pure beam. The direct design method results in significant crosstalk between OAM components within the beam. This is evident in the multiple intensity peaks and broader spectrum distribution. We also see strong interference from a zeroth-order component, especially in the beam center. These features highlight the limitations of the traditional direct approach.

In comparison, our nonlocal inverse design produces OAM beams with significantly reduced crosstalk. The desired OAM component is dominant in each graph, with less interference from other orders. The intensity distribution is more concentrated around the intended OAM order, indicating higher fidelity and purity. This improvement is particularly evident for higher-order OAM beams.

Figure 6 quantitatively compares the purity of OAM beams generated by both traditional direct and our inverse design methods using data from simulations and experiments. The vertical axis represents the OAM beam purity and the horizontal axis shows the OAM beam order. Beam purity refers to the percentage of energy carried by the desired OAM component compared with the total energy in the beam. A higher purity indicates a cleaner beam with less interference from undesired components.

The direct design method (blue crosses) results in lower OAM purity across all beam orders. The purity typically ranges between 70% and 89%, indicating a significant portion of energy in undesired components. This is particularly evident at higher-order OAM beams, where purity

drops further, which highlights the limitations of the traditional approach in controlling unwanted energy within the beam. In contrast, our inverse design method (red circles) achieves significantly higher purity, exceeding 90% for all OAM beam orders in both simulations and experiments. This high purity is maintained even for higher-order OAM beams, demonstrating the robustness of our inverse design approach in minimizing crosstalk and ensuring the desired OAM component dominates the beam. Compared with the direct method, this nonlocal design approach improves purity by up to 20%. This substantial enhancement signifies the superior performance of our inverse design method in generating cleaner beams with less interference. The consistency between simulation and experimental results further validates the effectiveness and practical applicability of our nonlocal inverse design methodology.

We further explore the robustness of our inverse design method under occlusion conditions and its capability to construct a composite OAM beam, which is difficult to address with conventional design methods. Figures 7(a) and 7(b) illustrate the influence of a $\pi/6$ occlusion on the radiation plane for generating OAM beams with $m = 2$. The direct design method shows significant degradation, introducing obvious unwanted OAM components. In contrast, the inverse design method optimizes the lens structure to mitigate the effects of occlusion, overcoming constraints and achieving superior performance. In addition, the construction of composite OAM beams holds valuable potential for acoustic manipulation and communication. As demonstrated in Figs. 7(c) and 7(d), the inverse design method effectively constructs a composite OAM beam with $m = 1$ and $m = 4$. The resulting spectrum is notably purer, exhibiting minimal mode crosstalk. In addition, the design achieves equal intensity for both $m = 1$ and
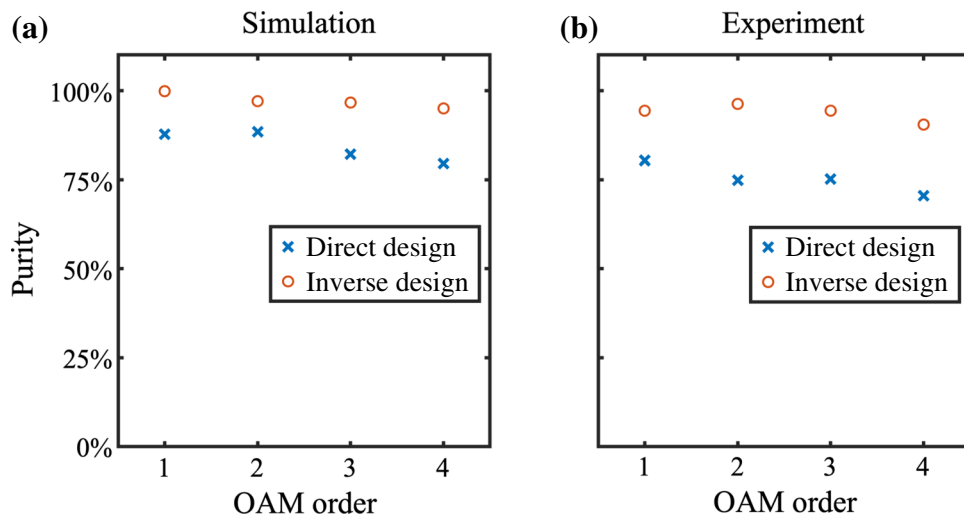

FIG. 6. Comparison of the purity of the OAM beams generated with the direct and our nonlocal inverse design methods from both the (a) simulations and (b) experiments.
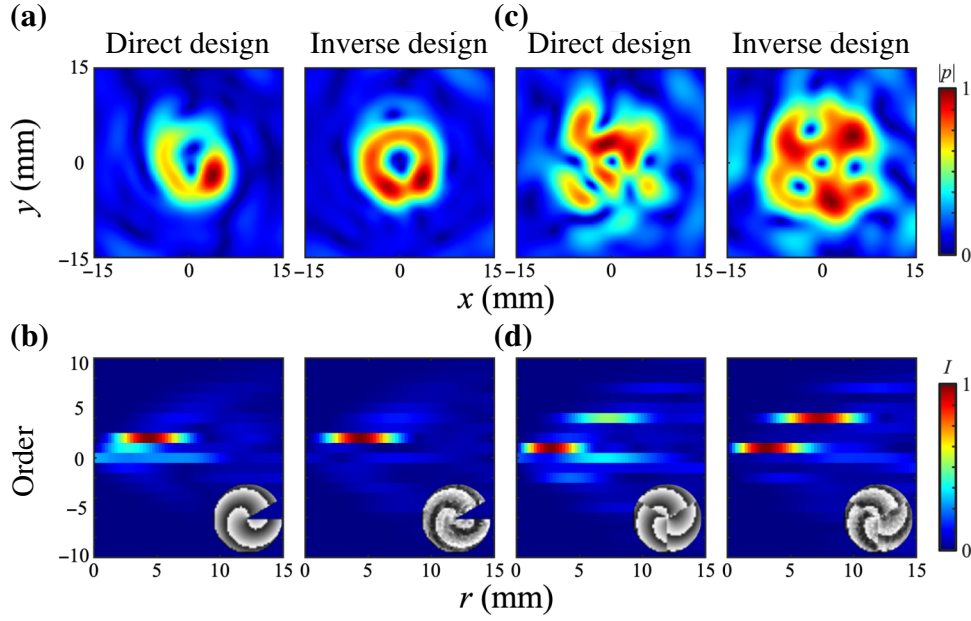
FIG. 7.   Comparison of the ultrasound OAM beams generated with the direct and nonlocal inverse design methods under occlusion and composite beam construction. (a) Ultrasound field distributions and (b) corresponding OAM spectra for an OAM beam with topological charge $m = 2$, subjected to a $\pi/6$ occlusion; inset displays the thickness profiles of the lenses. (c) Ultrasound field distribution and (d) corresponding OAM spectra for a composite OAM beam with $m = 1$ and $m = 4$.

$m = 4$ components, highlighting the method's precision and versatility.

The integration of a full-wave model with inverse design addresses the limitations of the traditional local design method, enabling the generation of high-purity OAM beams underwater. The inverse design method not only enhances purity but also introduces new possibilities for OAM construction, such as composite beams and maintaining purity under occlusion. These are challenges that conventional methods struggle to resolve. This is crucial for applications requiring a clear distinction between different OAM modes, such as underwater communication systems or detecting objects rotating underwater [38]. By concentrating energy in the desired mode, the nonlocal inverse design method reduces interference and enhances signal clarity, leading to more reliable and efficient operation in these applications.

IV. DISCUSSION

In conclusion, our nonlocal inverse design method represents a significant advancement in generating high-quality ultrasound OAM beams underwater by incorporating full-wave simulations throughout the inverse design process. This approach overcomes the limitations of traditional methods and leads to superior performance in both fundamental research and practical applications. The improvement in OAM purity, with values consistently exceeding 90%, ensures minimal crosstalk between different modes, which is critical for underwater communication

systems where high channel capacity and signal clarity are essential. In addition, the reduced crosstalk results in more reliable and efficient communication channels, which are essential for underwater sensor networks, autonomous underwater vehicles, and marine research.

The integration of full-wave models in the inverse design process could extend the applicability of OAM beams to more challenging environments, such as adapting to the density and sound speed variations of oceanic conditions and incorporating the complex environment of the human body into the lens design. This approach promises reliable communication and particle manipulation in deep-sea exploration and medical ultrasound applications. Our nonlocal inverse design method is not limited to generating high-purity OAM beams; it also enables the construction of complex sound fields, advancing various fields. For example, it can create multiple focal points within the body, enabling applications such as wireless charging of implanted medical devices with focused sound waves and precise neural modulation for targeted stimulation of specific areas of the nervous system. The efficiency of our method is enhanced by leveraging GPU acceleration to handle the computational complexity of full-wave simulations, balancing computational demands with high accuracy. The robustness of our method paves the way for new applications by enabling complex sound field constructions. Our comprehensive framework, built on full-wave simulations and accelerated through parallel computing, can be further enhanced by integrating deep learning algorithms. By enabling rapid predictions and

adjustments to various acoustic environments and requirements, deep learning can significantly streamline the optimization workflow [39,40]. This advancement would further solidify the practical applicability of our method in diverse real-world scenarios. Overall, our nonlocal inverse design method not only sets a new benchmark for generating high-purity OAM beams but also opens up new possibilities for various advanced acoustic technologies.

[1] C. Shi, M. Dubois, Y. Wang, and X. Zhang, High-speed acoustic communication by multiplexing orbital angular momentum, Proc. Natl. Acad. Sci. U. S. A. **114,** 7250 (2017).

[2] X. Jiang, B. Liang, J. C. Cheng, and C. W. Qiu, Twisted acoustics: metasurface-enabled multiplexing and demultiplexing, Adv. Mater. **30,** 1800257 (2018).

[3] A. E. Willner, K. Pang, H. Song, K. Zou, and H. Zhou, Orbital angular momentum of light for communications, Appl. Phys. Rev. **8,** 041312 (2021).

[4] S. Guo, X. Guo, X. Wang, X. Du, P. Wu, A. Bouakaz, and M. Wan, Manipulation of nanodroplets via a nonuniform focused acoustic vortex, Phys. Rev. Appl. **13,** 034009 (2020).

[5] Z. Gong and M. Baudoin, Three-dimensional trapping and assembly of small particles with synchronized spherical acoustical vortices, Phys. Rev. Appl. **14,** 064002 (2020).

[6] Y. Jia, S. Zhang, X. Zhang, H. Long, C. Xu, Y. Bai, Y. Cheng, D. Wu, M. Deng, and C.-W. Qiu, Compact meta-differentiator for achieving isotropically high-contrast ultrasonic imaging, Nat. Commun. **15,** 2934 (2024).

[7] Q. Feng, X. Kong, M. Shan, Y. Lin, L. Li, and T. J. Cui, Multi-orbital-angular-momentum-mode vortex wave multiplexing and demultiplexing with shared-aperture reflective metasurfaces, Phys. Rev. Appl. **17,** 034017 (2022).

[8] X.-R. Li, J.-J. Feng, B.-C. Ping, Y. Sun, D.-J. Wu, and B. Assouar, Periodic-phase acoustic vortices with tunable comblike orbital angular momentum spectrum, Phys. Rev. Appl. **20,** 034008 (2023).

[9] Y. Jia, Y. Liu, B. Hu, W. Xiong, Y. Bai, Y. Cheng, D. Wu, X. Liu, and J. Christensen, Orbital angular momentum multiplexing in space–time thermoacoustic metasurfaces, Adv. Mater. **34,** 2202026 (2022).

[10] K. Wu, J.-J. Liu, Y.-j. Ding, W. Wang, B. Liang, and J.-C. Cheng, Metamaterial-based real-time communication with high information density by multipath twisting of acoustic wave, Nat. Commun. **13,** 1 (2022).

[11] C. Zhang, X. Jiang, J. He, Y. Li, and D. Ta, Spatiotemporal acoustic communication by a single sensor via rotational Doppler effect, Adv. Sci. **10,** 2206619 (2023).

[12] B. T. Hefner and P. L. Marston, An acoustical helicoidal wave transducer with applications for the alignment of ultrasonic and underwater systems, J. Acoust. Soc. Am. **106,** 3313 (1999).

[13] K. Volke-Sepúlveda, A. O. Santillán, and R. R. Boullosa, Transfer of angular momentum to matter from acoustical vortices in free space, Phys. Rev. Lett. **100,** 024302 (2008).

[14] A. Anhäuser, R. Wunenburger, and E. Brasselet, Acoustic rotational manipulation using orbital angular momentum transfer, Phys. Rev. Lett. **109,** 034301 (2012).

[15] C. E. Demore, Z. Yang, A. Volovick, S. Cochran, M. P. MacDonald, and G. C. Spalding, Mechanical evidence of the orbital angular momentum to energy ratio of vortex beams, Phys. Rev. Lett. **108,** 194301 (2012).

[16] A. Marzo, S. A. Seah, B. W. Drinkwater, D. R. Sahoo, B. Long, and S. Subramanian, Holographic acoustic elements for manipulation of levitated objects, Nat. Commun. **6,** 8661 (2015).

[17] M. Baudoin, J.-C. Gerbedoen, A. Riaud, O. B. Matar, N. Smagin, and J.-L. Thomas, Folding a focalized acoustical vortex on a flat holographic transducer: Miniaturized selective acoustical tweezers, Sci. Adv. **5,** eaav1967 (2019).

[18] Z. Gao, S. Wang, Y. Sui, Q. Zhang, Y. Yang, J. Huang, Y. Xiong, T. Ma, X. Zhang, and H. Zheng, A multifunctional acoustic tweezer for heterogenous assembloids patterning, Small Struct. **4,** 2200288 (2023).

[19] C. Zhang, X. Jiang, S. Han, J. He, Y. Zheng, B. Li, and D. Ta, Converged wireless infrastructure with acoustic holographic array, Appl. Phys. Rev. **9,** 041413 (2022).

[20] X. Jiang, Y. Li, B. Liang, J.-c. Cheng, and L. Zhang, Convert acoustic resonances to orbital angular momentum, Phys. Rev. Lett. **117,** 034301 (2016).

[21] X. Jiang, J. He, C. Zhang, H. Zhao, W. Wang, D. Ta, and C.-W. Qiu, Three-dimensional ultrasound subwavelength arbitrary focusing with broadband sparse metalens, Sci. China: Phys., Mech. Astron. **65,** 224311 (2022).

[22] B. Assouar, B. Liang, Y. Wu, Y. Li, J.-C. Cheng, and Y. Jing, Acoustic metasurfaces, Nat. Rev. Mater. **3,** 460 (2018).

[23] H.-T. Zhou, W.-X. Fu, Y.-F. Wang, and Y.-S. Wang, High-efficiency ultrathin nonlocal waterborne acoustic metasurface, Phys. Rev. Appl. **15,** 044046 (2021).

[24] J. He, X. Jiang, H. Zhao, C. Zhang, Y. Zheng, C. Liu, and D. Ta, Broadband three-dimensional focusing for an ultrasound scalpel at megahertz frequencies, Phys. Rev. Appl. **16,** 024006 (2021).

[25] L. Fan and J. Mei, Multifunctional waterborne acoustic metagratings: From extraordinary transmission to total

and abnormal reflection, Phys. Rev. Appl. **16,** 044029 (2021).

[26] K. Melde, A. G. Mark, T. Qiu, and P. Fischer, Holograms for acoustics, Nature **537,** 518 (2016).

[27] Z. Hou, H. Ding, N. Wang, X. Fang, and Y. Li, Acoustic vortices via nonlocal metagratings, Phys. Rev. Appl. **16,** 014002 (2021).

[28] W. W. Ahmed, M. Farhat, X. Zhang, and Y. Wu, Deterministic and probabilistic deep learning models for inverse design of broadband acoustic cloak, Phys. Rev. Res. **3,** 013142 (2021).

[29] Z. Du and J. Mei, Metagrating-based acoustic wavelength division multiplexing enabled by deterministic and probabilistic deep learning models, Phys. Rev. Res. **4,** 033165 (2022).

[30] Q. Wang, M. Fink, and G. Ma, Maximizing focus quality through random media with discrete-phase-sampling lenses, Phys. Rev. Appl. **19,** 034084 (2023).

[31] L. Fan and J. Mei, Metagratings for waterborne sound: Various functionalities enabled by an efficient inverse-design approach, Phys. Rev. Appl. **14,** 044003 (2020).

[32] Z.-x. Xu, B. Zheng, J. Yang, B. Liang, and J.-c. Cheng, Machine-learning-assisted acoustic consecutive Fano resonances: Application to a tunable broadband low-frequency metasilencer, Phys. Rev. Appl. **16,** 044020 (2021).

[33] K. Deb, A. Pratap, S. Agarwal, and T. Meyarivan, A fast and elitist multiobjective genetic algorithm: NSGA-II, IEEE Trans. Evol. Comput. **6,** 182 (2002).

[34] B. E. Treeby and B. T. Cox, k-Wave: MATLAB toolbox for the simulation and reconstruction of photoacoustic wave fields, J. Biomed. Opt. **15,** 021314 (2010).

[35] B. E. Treeby, J. Jaros, D. Rohrbach, and B. Cox, in *2014 IEEE International Ultrasonics Symposium* (IEEE, 2014), p. 146.

[36] B. Jack, M. Padgett, and S. Franke-Arnold, Angular diffraction, New J. Phys. **10,** 103013 (2008).

[37] C. Zhang, J. He, X. Jiang, and D. Ta, Inverse-design methodology for generating twisted ultrasonic motor in free space, Adv. Intell. Syst. **5,** 2300255 (2023).

[38] C. Zhang, X. Jiang, and D. Ta, Revealing the incidence-angle-independent frequency shift in the acoustic rotational Doppler effect, Phys. Rev. Lett. **132,** 114001 (2024).

[39] K. Donda, Y. Zhu, A. Merkel, S. Wan, and B. Assouar, Deep learning approach for designing acoustic absorbing metasurfaces with high degrees of freedom, Extreme Mech. Lett. **56,** 101879 (2022).

[40] Z. Du and J. Mei, Wide-angle and high-efficiency acoustic retroreflectors enabled by many-objective optimization algorithm and deep learning models, Phys. Rev. Mater. **7,** 115201 (2023).